Computational Modeling of Natural Gas Production From Hydrate Dissociation

Goodarz Ahmadi

Department of Mechanical and Aeronautical Engineering
Clarkson University, Potsdam, NY 13699-5725

Abstract

This paper provides an overview of computational modeling of hydrate dissociation. A simplified axisymmetric model for natural gas production from the dissociation of methane hydrate in a confined reservoir by a depressurizing well was first described. During the hydrate dissociation, the heat and mass transfer in the reservoir were analyzed, assuming a sharp dissociation front. The system of governing equations was solved by a finite difference scheme, and the distributions of temperature and pressure in the reservoir, as well as the natural gas production from the well were evaluated. The numerical results were compared with those obtained by the linearization method.

Hydrate dissociation in a porous sandstone core was then studied using a kinetic model. The ANSYS-FLUENT code was used for analyzing hydrate dissociation in an axisymmetric core. When the core was opened exposing the core to low pressure, the hydrate in the core dissociates and the methane gas and liquid water begin to flow in the pores. A Users' Defined function (UDF) for analyzing hydrate dissociation was developed and included in the FLUENT code. The New UDF used the Kim-Bishnoi kinetic model for hydrate dissociation. Variations of relative permeability of the core were included in the model. Sample simulation results were presented and discussed.

1. Introduction

Gas hydrates (gas clathrates) are solid compounds of natural gas molecules that are encaged within a crystal structure composed of water molecules. Hydrates are formed under certain thermodynamically favorable conditions. Physical appearance of gas hydrates resemble packed snow or ice (Sloan, 1998). According to Makogon (1997), there are tremendous amounts of natural gas trapped in hydrates in arctic regions and in the continental shelves beneath the oceans around the globe.

Per unit volume, gas hydrates contain a tremendous amount of natural gas. According to Kvenvolden (1993), 1 m3 of hydrate dissociating at atmospheric temperature and pressure forms 164 m3 of natural gas and 0.8 m3 of water.

Thus, developing methods for commercial production of natural gas from hydrates have attracted considerable attention in the recent years. Extensive reviews of properties of hydrates were provided by Sloan (1998), Makogon (1974, 1997) and Englezos (1993).

Accordingly, hydrate dissociates when its phase equilibrium breaks down due to increase in temperature or reduction in pressure.

In the 1960s, natural gas hydrate reservoirs were discovered in oceanic sediment and in permafrost regions of the earth (Katz, 1971, Makogon, 1966). World reserves of natural gas trapped in hydrate state have been estimated to be several times the known reserves of conventional natural gas and oil combined (Makogon, 1997; Kvenvolden, 1993, MacDonald, 1990b). Therefore, hydrate has the potential to become a major source of energy in the second half of the 21st century. Thus, developing methods for commercial production of natural gas from hydrates has attracted considerable attention (Collett, 1993, 1997, 2002; Kvenvolden, 1993; Milkov and Sassen, 2003). Recent years has seen considerable efforts for commercial production of natural gas from hydrate reservoirs. However, most of the efforts have been limited to laboratory and bench-scale studied. According to Makogon (1997) natural gas production was exploited successfully at the gas-hydrate field in Western Siberia.

Blockage of flow lines and gas pipelines in Arctic regions can occur due to gas-hydrate formation (Sloan, 1998). Behar et al. (1994), Yousif and Dunayevsky (1997), Paez et al. (2001) and Reyma and Stewart (2001) described different methods for preventing hydrate formation in petroleum production and transportation equipment and/or to remove hydrate plug in oil and gas pipelines.

Methane is a greenhouse gas and massive dissociation of hydrates could cause climate change and a global warming. This process is believed to have influenced past climate changes (MacDonald, 1990a; Kvenvolden, 1991; Englezos and Hatzikiriakos, 1994; Henriet, 1998; Haq, 1998; Hesselbo et al., 2000).

Natural gas production from hydrate can occur by depressurization, thermal stimulation, and inhibitor injection. In depressurization technique, a well is drilled into the hydrate reservoir lowering the pressure to below the thermodynamic equilibrium condition causing hydrate to dissociate. In this case, however, the heat of dissociation must be supplied from the surrounding formation (Selim et al., 1990; Hong et al., 2003a,b).. The presence of a free-gas zone beneath hydrate may be essential to the success of the depressurization method. The most common depressurization technique is drilling through the hydrate layer and completing the well in the free-gas zone. Gas production from this layer leads to pressure reduction and dissociation of the overlying hydrate supplies the reservoir with fresh natural gas. Makogon (1981) discussed gas production from the Messoyakha field based on this depressurization technique. Collett et al. (1998) and Kamath (1998) suggested that the depressurization method is the most economically feasible approach.

There have been a number of studies on simulating the gas hydrate dissociation and formation process. Holder et al. (1982) reported that the energy value of the produced gas is roughly 10 times the energy required to dissociate hydrate in typical reservoirs. Englezos and Bishnoi (1988) described the formation of gas hydrates in solutions of aqueous electrolytes. Sun and Mohanty (2006) simulated the formation and dissociation of methane hydrate in porous media.

Ji et al. (2001, 2003) presented a parametric study of natural gas production from the dissociation of methane hydrate in a confined reservoir using depressurization method. The one-dimensional linearized model suggested by Makogon (1997) was used in the analysis. They showed that the gas production rate was a sensitive function of well pressure, reservoir temperature and zone permeability.

Ahmadi et al. (2004, 2007) described one-dimensional and axisymmetric computational models for natural gas production from the dissociation of methane hydrate in a confined

reservoir by a depressurizing well. They accounted for the dissociation heat absorption and solved the convection–conduction heat transfer in the gas and hydrate zones. It was shown that the gas production rate was a sensitive function of well pressure.

Vysniauskas and Bishnoi (1983) performed a series of studies of the kinetics of gas hydrate formation. Isothermal and isobaric experiments were carried out in a semi-batch stirred tank reactor using methane and ethane. Englezos et al. (1987) related the gas consumption rate with hydrate crystal growth rate. Their experimental data suggested that the rate constants have weak dependence on the temperature. Kim et al. (1987) developed a model to describe the kinetics of methane hydrate dissociation. The model assumed that, at a constant temperature, a two-step process could describe gas hydrate dissociation; the first is the destruction of the clathrate host lattice at the surface of a particle and the second step is desorption of the guest molecule from the surface. These steps occur at the solid surface, not within the bulk of hydrate.

The so-called Kim-Bishnoi kinetic model developed by Kim et al. (1987) was used in several studies in the past. Masuda et al. (1999) formed methane hydrate in a core-shape vessel and measured the amount of gas generation due to hydrate dissociation using a depressurization method. They also performed a computer model study and compared their simulation results with the experimental data for different cases. Later, Clarke and Bishnoi (2000 and 2001) measured the rate of decomposition of gas hydrates formed from mixtures of methane and ethane.

Moridis et al. (2005) reported the results of their computer model for the gas generation in a hydrate core due to dissociation by heating. They also compared their numerical simulation results with the experimental data of Kneafsey et al. (2005).

In this study, the computational models for analyzing hydrate dissociation are described. In the first approach it is assumed that there is sharp front for hydrate dissociation. Attention was given to the potential for natural gas production from hydrate reservoir by depressurization. When a well is drilled into a hydrate reservoir, the pressure decreases to below the thermodynamics equilibrium pressure for hydrate at a specified temperature. Thus, the hydrate will dissociate and natural gas is released. It is assumed that the reservoir is partially saturated with hydrate and contains pressurized, free natural gas. It is also assumed that the well is kept at a constant pressure. The presented axisymmetric model includes the energy and mass balance at the dissociation front and accounts for heat conduction in the hydrate zone of the reservoir. The resulting system of coupled governing equations is solved using a finite-difference numerical scheme in conjunction with an iterative procedure. Numerical solutions for time evolutions of pressure and temperature profiles in the hydrate reservoir, as well as the location of the dissociation front are obtained for several well pressures and reservoir temperatures. The simulation results are compared with those obtained earlier by a linearization approach. It is shown that the natural gas production rate is a sensitive function of well pressure and reservoir temperature.

For the second computational model, the dissociation of methane hydrate in a core is studied. It was assumed that the pores of the core are partially saturated with hydrate. An axisymmetric computer model of the hydrate core is developed and solved for the multiphase flow and thermal field during the hydrate dissociation using the ANSYS-FLUENT code augmented with specially developed hydrate modules user defined Functions (UDF). The user defined programs accounts for the dissociation process of hydrate including the rate of dissociation, the heat absorbed, and the amounts of generated gas and water. The UDFs also include the effects of relative permeability of water and gas and effective porosity of the core.

For different core initial temperatures and various outlet valve pressures, time evolutions of temperature and pressure profiles, as well as the cumulative amount of natural gas produced are evaluated. The simulation results show that the process of natural gas production is a sensitive function of temperature and pressure, as well as core permeability. The simulation results are compared with available experimental data and qualitative agreement is found.

2. Axisymmetric Model

Consider an unbounded methane hydrate reservoir underground that is partially saturated with solid hydrate and also contains pressurized natural gas at the reservoir pressure P_e and reservoir temperature T_e. At this reservoir pressure, the hydrate must be stable, with $P_e > P_D$, where P_D is the hydrate dissociation pressure at dissociation temperature T_D. When a well is drilled into the reservoir, the pressure in the well drops to less than P_D; the hydrate near the well becomes unstable and dissociates into natural gas and water. The process of hydrate dissociation then expands radially outward from the well with time. In this approach, it is assumed that the hydrate dissociation occurs in a narrow region, which can be treated as the dissociation front. This moving cylindrical front separates the volume of the reservoir into two zones with different phases. The near-well gas-zone contains free natural gas and liquid water, while the hydrate-zone beyond the dissociation front contains the solid hydrate and free natural gas. Pressures and temperatures in these two zones gradually decrease, as the natural gas flows towards the well, while the dissociation front moves away from the well.

Here it is assumed that the temperature and pressure distributions are axisymmetric with respect to the well centerline. The dissociation front is also a cylinder with its axis at the well. The pressure and temperature at the dissociation front are the equilibrium pressure, P_D, and temperature, T_D, both of which are functions of time.

Figure 1 shows the axisymmetric model used in the computation. In this figure, the well radius is r_0 and a cylindrical part of the reservoir with a radius of L = 100 m is analyzed. The computation domain ranges from $r=r_0$, where the well pressure is fixed at P_G, to r = L the reservoir pressure and temperature are, respectively, fixed at Pe and Te.

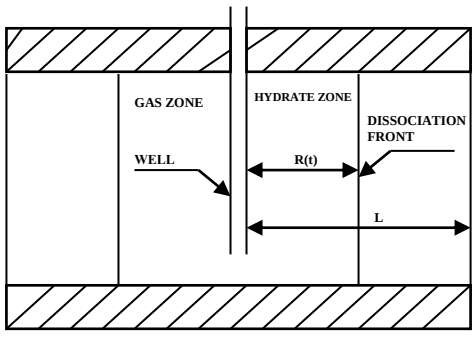

Figure 1. Schematics of the hydrate reservoir for the axisymmetric model.

In Figure 1, the dissociation front, which is located at R(t), separates the reservoir into two zones. The region $r_o < r < R(t)$ is referred to as the gas zone, and the area R(t) < r < L is the hydrate zone. The dissociation front R(t) moves outward as the gas production from the well continues.

In the subsequent analysis, subscript *n* identifies the regions, with *n* = 1 or 2 corresponding to the gas zone or the hydrate zone respectively. Pressure distribution in the reservoir is governed by:

$$\frac{\partial P_n}{\partial t} = a_n \frac{1}{r}\frac{\partial}{\partial r}(r\frac{\partial P_n^2}{\partial r}) \quad (1)$$

where

$$a_n = \frac{k_n}{\Phi_n \mu} \quad (2)$$

and

$$\Phi_1 = (1-\alpha)\,\Phi \quad (3)$$

$$\Phi_2 = (1-\beta)\,\Phi \quad (4)$$

Here P_n and k_n are the pressure and the gas permeability, respectively, μ is the gas viscosity, α is the water saturation, β is the hydrate saturation, Φ is the porosity, Φ_1 is the content of free gas in the gas zone, and Φ_2 is the content of free gas in the hydrate zone.

The velocity of natural gas v_n in the gas and the hydrate zones is given by Darcy's law. i.e.,

$$v_n = -\frac{k_n}{\mu}\frac{\partial P_n}{\partial r} \quad (5)$$

Assuming that the time variation of gas density is small, the heat transfer equation in the gas zone is given as

$$\frac{\partial T_1}{\partial t} + v_1 \frac{\partial T_1}{\partial r} = 0 \quad (6)$$

where T_1 is the temperature, and v_1 is the velocity of natural gas in the gas zone. Here heat conduction in the gas zone, which is much smaller than the heat convection, is neglected.

The heat transfer equation in the hydrate zone is given as

$$\frac{\partial T_2}{\partial t} + v_2 \frac{\partial T_2}{\partial r} = \alpha_2 \frac{1}{r}\frac{\partial}{\partial r}(r\frac{\partial T_2}{\partial r}) \quad (7)$$

where α_2 is heat diffusivity in the hydrate zone.

In general, the equilibrium temperature and pressure at the dissociation front are functions of time. The phase equilibrium relation between temperature T_D and pressure P_D at the dissociation front is given as (Makogon, 1997)

$$\log_{10} P_D = A_b (T_D - T_0) + B_b (T_D - T_0)^2 + C_b \quad (8)$$

where T_0 is 273.15K and a,b,c are empirical constants that depend on the hydrate composition. Values of a, b, and c are obtained from the equilibrium pressure-temperature data of methane hydrate. Using the least square fit method, it follows that (Ji et al. 2001)

$$A_b = 0.0342\ K^{-1},\ B_b = 0.0005\ K^{-2},\ C_b = 6.4804$$

where in Equation (8) P_D is in Pa.

The process of hydrate dissociation at the dissociation front is an endothermic phase-change process. The dissociation heat per kilogram of hydrate in J/kg is given as (Kamath, 1983)

$$\Delta H = AT_D + B \quad (9)$$

where T_D is the dissociation temperature, and A, B are constants given by

$$A=-1050\ J/kg,\quad B=3527000\ J/(kgK)$$

These together with the appropriate equations of balance of mass and heat flow at the dissociation front form the set of governing equations for the gas flow and the pressure and thermal condition in the hydrate reservoir.

Equations (1), (6), (7) are three coupled equations governing the temperature and pressure variations in the reservoir. These equations are non-dimensionalized and solved with a finite difference method. An explicit central difference method is used to solve Equation (1) for the pressure and an upstream explicit method is used to solve the convection heat transfer equation in the gas zone given by Equation (6). To solve the conduction-convection heat transfer equation in the hydrate zone given by (7), an implicit method is used. Additional details of the computational model were described by Ji et al. (2002).

3. Axisymmetric Well Results

This section presents sample numerical solution results for time evolutions of pressure and temperature profiles in the hydrate reservoir under various conditions. In addition, time variations of methane gas production and location of the dissociation front are also evaluated. For a reservoir temperature of 287 K, reservoir pressure of 15 MPa and a well pressure of 2 MPa, Figure 2 shows variations of pressure and temperature profiles at different times. In this case phase permeability in the hydrate and the gas zones are, respectively, 1 md and 8 md. Figure 2a shows that the temperature profiles in the hydrate and gas zones are quite different. In the hydrate zone, the temperature decreases gradually from reservoir temperature far from the front to the dissociation temperature at the front. In the region near the dissociation front, the gradient of temperature variation becomes sharp, which leads to a sharply increasing heat conduction to the front. In the gas zone, temperature varies very smoothly from the dissociation temperature at the dissociation front to its minimum value at the well. For different times, the temperature profiles from the well to the dissociation front are nearly the same. Figure 2a also shows that the temperature at the dissociation front, T_D, increases gradually with time as the dissociation front moves outward.

The corresponding pressure profiles for different times under the same conditions are presented in Figure 2b. The pressure decreases gradually from the reservoir pressure to the dissociation pressure at the dissociation front, and then decreases in the gas zone. In the region near the well, pressure drops sharply to the well pressure. At the dissociation front, a slope change of pressure profiles is observed, which is due to the large difference of phase permeability in the gas zone and hydrate zone in this case.

In Figure 2c, time evolutions of the gas mass flow ($2\pi r\rho v$) across the reservoir are displayed. It is seen that the mass flow is nearly fixed in both the gas zone and the hydrate zone. There is a jump in the mass flow due to the hydrate dissociation, which moves outwards with time as the dissociation front penetrates deeper in the hydrate reservoir. It is also noticed that the gas mass flow in the reservoir and the amount of natural gas generated due to hydrate dissociation increase gradually with time.

Figure 2d presents the heat flow profiles throughout the reservoir at different times. The solid line in this figure shows the profile at 10 days, while the 40-day profile is shown by a dashed line. It is seen that in the gas zone, where only the convective heat transfer is considered, the heat flow is nearly the same. In the hydrate zone far from the dissociation front, the heat flow--which is primarily convective heat flow--is roughly constant. Near the front region, as the temperature decreases sharply to the dissociation temperature at the front, the heat conduction becomes quite large and the total heat flow increases sharply to the maximum value at the dissociation front. There is a jump of heat flow at the dissociation

front, which supplies the heat needed for hydrate dissociation. Figure 2d also shows that the total heat flow increases with time.

Comparisons of temperature, pressure and gas flow profiles as predicted by the numerical method used in this paper with the linearization method suggested by Makogon (Ji et al. 2001) are presented in Figure 3. Here a reservoir temperature of 287 K, a reservoir pressure of 15 MPa and a well pressure of 2 MPa are used and all other parameters are kept identical. In these figures, results of the numerical method are shown by the solid lines, while those of the linearized method are shown by the dashed lines. Although (not shown) both temperature profiles reach the same boundary condition far from the front, from Figure 3a it is seen that near the dissociation front the temperature profiles of the numerical method have much sharper gradients when compared with those of the linearization method. The reason is that in linearization method suggested by Makogon the heat conduction was ignored.

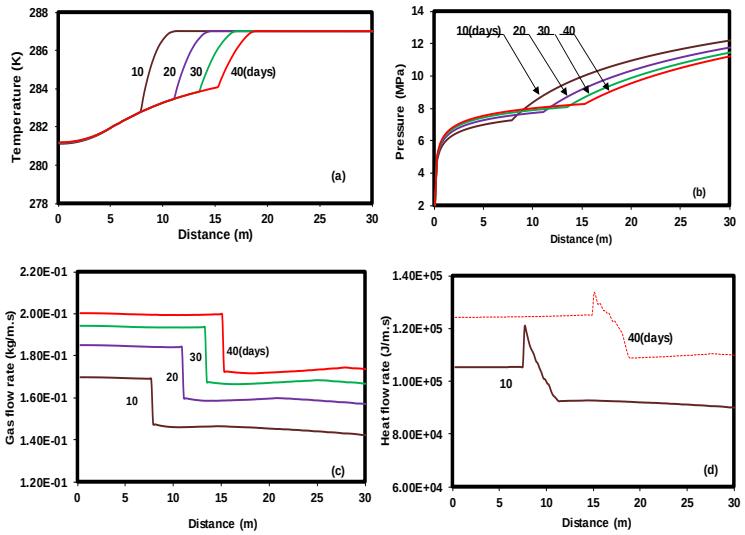

Figure 2. Time variations of pressure, temperature, gas mass flow and heat flow profiles in a reservoir for a well pressure of 2MPa and a reservoir temperature of 287K.

To display the role of various heat flows at the dissociation front, (a) time variations of conductive heat flow into the dissociation front, and (b) convective heat flows into and out of the dissociation front are shown in Figure 3b. It is clear that the convective heat flow into the dissociation front is roughly equal to the convective heat flow out of the front. This means that the conductive heat flow plays the dominant role in supplying the heat for hydrate dissociation. Figure 3b further implies that without the heat conduction, the energy balance at the dissociation front cannot be satisfied.

Figure 3c compares the present pressure profiles with those obtained by the linearization method. It is seen that the pressure profiles are qualitatively comparable. Pressure as predicted by the linearization method is lower than that of the numerical method. The main reason is that in the linearization method, Equation (1) is linearized with reservoir pressure P_e in the hydrate zone or well pressure P_G in the gas zone. This causes the dissociation pressure obtained from the linearization method to be lower than that of the numerical method.

Comparison of the mass flow ($2\pi r\rho\upsilon$) profiles as obtained by the numerical and the linearization methods is shown in Figure 3d. It is seen that for both methods, the trends of

mass flow profiles throughout the reservoir are similar. However, mass flow of the linearization method is lower than that of the numerical method. The reason is that the velocity as given by Darcy's law is proportional to the pressure gradient, and density is proportional to the ratio of pressure over temperature. At a fixed time, Figure 3 shows that the temperatures predicted by the numerical method are higher than those estimated by the linearization method. Furthermore, the predicted pressure gradient in the hydrate zone is larger than that of the linearization method. The combined effects of a larger pressure gradient and a higher temperature and pressure of the numerical method lead to a higher mass flow throughout the reservoir.

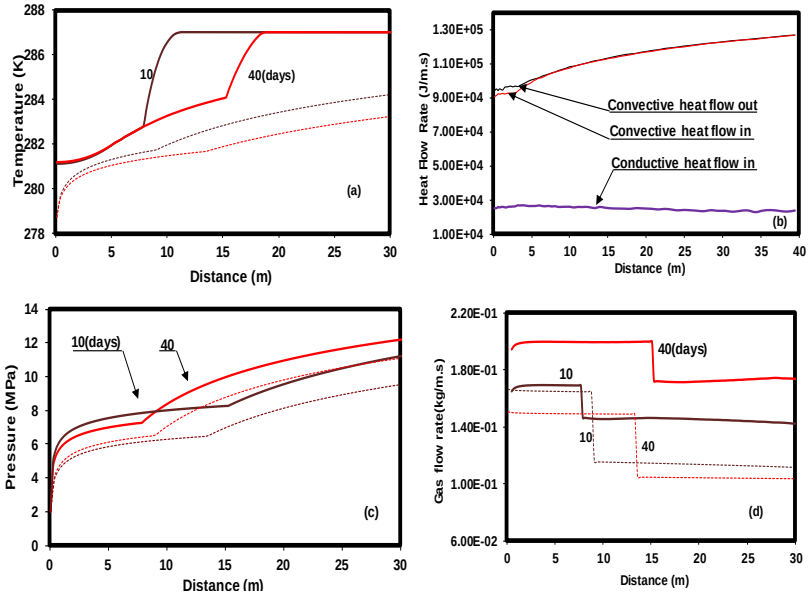

Figure 3. Comparison of the present temperature and pressure profiles and mass flow rate with linearized solutions for a reservoir temperature of 287K and a well pressure of 2MPa. Solid lines: numerical solutions. Dashed lines: linearized solutions suggested by Makogon (Ji et al., 2001).

Time variations of movement of dissociation front, gas mass flow at the well and dissociation temperature for different well pressures as obtained by the present numerical method are compared with those of the linearization approach (Makogon, 1997, Ji et al., 2001) in Figure 4. Here the reservoir conditions are kept fixed at 15 MPa and 287 K. The permeabilities in gas and hydrate zones are, respectively, 8 md and 1 md. In this figure, numerical solutions are shown by solid lines, while the linearized solutions are shown by dashed lines. Figure 4a shows that the distance of the front from the well increases with time. As the well pressure increases, the outward motion slows down. It is observed that for the linearization method, predicts a more sensitive motion of the dissociation front with the well pressure when compared with that of the numerical method.

Time evolutions of the natural gas output are displayed in Figure 4b. For a fixed well pressure and large time the present numerical predicts a large gas output compared to the linearization method. It is also seen that the natural gas output obtained the numerical method increases with time, and it trends to reach a constant value at large time. The gas output as evaluated by the linearization method, however, decreases with time and approaches a constant value at large time.

As was noted before, the present method leads to dissociation temperatures and pressures that are functions of time. Figure 4c shows time variations of the dissociation temperature for

different well pressures. It is seen that for a fixed well pressure, the dissociation temperature of the numerical method increases with time. (The slight fluctuation of the dissociation temperature at the beginning is related to the assumed initial start up conditions in the reservoir.) The dissociation temperature of the numerical method also varies with the well pressure, and increases as the well pressure increases. For the linearization method, however, the dissociation temperature varies with time very slightly, and is not as sensitive to well pressure to the extent predicted by the numerical method.

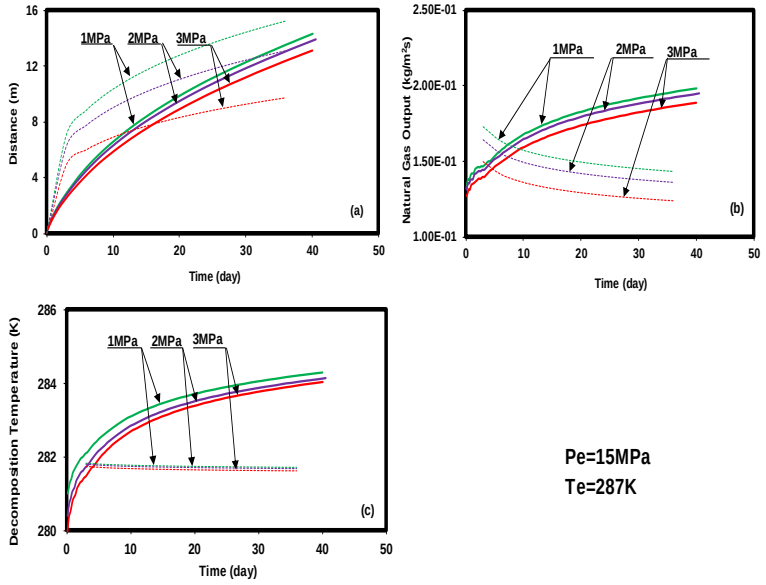

Figure 4. Comparison of present time variations of the position of dissociation front, natural gas output and dissociation temperature with linearized solutions for different well pressures. Solid lines: numerical solutions; Dashed lines: linearized solutions suggested by Makogon (Ji et al., 2001).

For different reservoir temperatures, Figure 5 compares time variations of the movement of the dissociation front, natural gas output and the dissociation temperature as predicted by the numerical method with those of the linearization approach. Here the reservoir and well pressures of 15MPa and 2MPa are assumed and the values of all other parameters are kept the same as those used in Figure 4. Figure 5a shows that the dissociation front moves faster when the reservoir temperature increases. The linearization method, however, predicts a sharper variation of the dissociation front motion when compared with the numerical method.

Figure 5b displays time variations of the natural gas output for different reservoir temperatures. The natural gas output increases with reservoir temperature. The numerical method leads to an increasing trend of natural gas output with time, while the linearization approach predicts a decreasing trend. It also observed that the long-term natural gas output predicted by the linearization method is lower than that of the numerical method for the same reservoir temperature.

Figure 5c shows time variations of the dissociation temperature with the reservoir temperature. The numerical method predicted that the dissociation temperature increases with time and the reservoir temperature. The linearization approach leads to only slight variations of the dissociation temperatures.

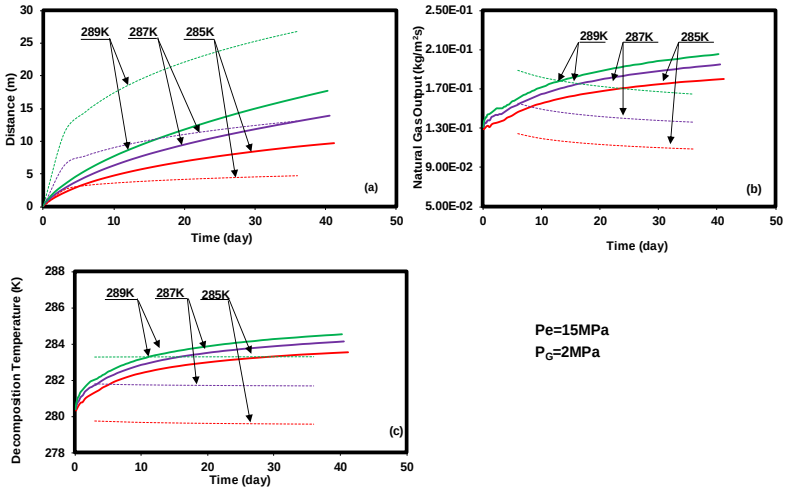

Figure 5. Comparison of the present time variations of the position of dissociation front, natural gas output and dissociation temperature with linearized solutions for different reservoir temperatures. Solid lines: numerical solutions; Dashed lines: linearized solutions suggested by Makogon (Ji et al., 2001).

4. Hydrate Core Model

The governing equations used to solve for the multiphase flow conditions during the hydrate dissociation process are outlined in this section. The continuity equations for different species are given by

$$-\nabla\cdot\rho_k\mathbf{u}_k+\dot{m}_k=\frac{\partial}{\partial t}\left(\phi_o\rho_k S_k\right),\ (k=H,g,w) \tag{10}$$

where $\dot{m}_k$ is the rate of generation/dissociation of species *k*, ϕ_o is the porosity of the core, S_k is the saturation of phase k, ρ_k is the phase density, t is time, and $\mathbf{u}_k$ is fluid velocity vector (with $\mathbf{u}_H=0$ since hydrate is stationary). Here *H*, *g* and *w* stand for hydrate, gas and water phases.

For saturations of various phases, the following equality holds

$$S_g+S_w+S_H=1, \tag{11}$$

where $S_g, S_w,$ and S_H are, respectively, saturation of gas, water and hydrate phases. The effective porosity of the medium is given as,

$$\phi_{eff}=\phi_o(1-S_H). \tag{12}$$

The Darcy's law for flow in porous media is given by

$$u_k=-\frac{K_D K_{rk}}{\mu_k}\nabla p,(k=g,w), \tag{13}$$

where K_{rk} is relative permeability of phase k and μ_k is the phase viscosity. Here, K_D is the absolute permeability of the media and is modeled as (Masuda et al., 1999)

$$K_D=K_{Do}(1-S_H)^N, \tag{14}$$

where K_{Do} is the absolute permeability at zero hydrate saturation, and N is the permeability reduction index which depends on the pore structure of the medium. Note that Equation (5) satisfies the expected limiting conditions at $S_H=0$ or 1, and the value of the permeability index N is determined experimentally.

The relative permeability of water and gas are evaluated by Corey's (1954) formula given as,

$$K_{rw} = \bar{S}^4, \tag{15}$$

and

$$K_{rg} = (1-\bar{S})^2(1-\bar{S}^2), \tag{16}$$

where

$$\bar{S} = \frac{S_w - S_{wr}}{1 - S_{gr} - S_{wr}}. \tag{17}$$

In Equations (13) to (17), K_{rw} and K_{rg} are, respectively, the relative permeability of water and gas, and S_{wr} and S_{gr} are the saturations of water and gas.

The equation of energy balance for the effective medium may be written as

$$\frac{\partial}{\partial t}\left[(1-\phi_o)\rho_R C_R T + \phi_o S_H \rho_H C_H T + \phi_o S_w \rho_w U_w + \phi_o S_g \rho_g U_g\right] = \nabla\cdot(K_o \nabla T) - \nabla\cdot\left(\rho_w h_w \mathbf{u}_{D,w} + \rho_g h_g \mathbf{u}_{D,g}\right) - \dot{Q}_H \tag{18}$$

where T is the temperature, C is the heat capacity, U is the internal energy, and h is the enthalpy. Subscripts R, H, w and g, respectively, indicate rock, hydrate, water and gas. Here, K_o is the effective thermal conductivity and is defined as

$$K_o = (1-\phi_o)K_R + \phi_o(S_H K_H + S_g K_g + S_w K_w), \tag{19}$$

where $K_R, K_H, K_g,$ and K_w, are respectively, thermal conductivity of rock, hydrate, gas and water. In Equation (18), $\dot{Q}_H$ is heat-sink/source rate due to hydrate dissociation.

Kim et al. (1986) developed a model for the molar generation rate of methane gas due to hydrate dissociation, $\dot{n}_{gp}$. Accordingly,

$$\dot{n}_{gp} = k_B A_p [P_e(T) - P] \tag{20}$$

$$k_B = k_d^o \exp\left(-\frac{\Delta E}{RT}\right) \tag{21}$$

where *Pe* is the equilibrium pressure, *P* is the local pressure in the core and *Ap* is the surface area of hydrate per unit volume. The surface area of hydrate particles was expressed as function of moles of hydrate assuming that hydrate density and composition was invariant. This model is referred to as the Kim-Bishnoi model. The dissociation rate constant, k_B, is given by Equation (21), where ΔE is the activation energy, R is the gas constant, and T is the temperature. The constant k_d^o is an intrinsic dissociation constant and is independent of pressure and temperature. In practice, these parameters are evaluated by curve fit to the experimental kinetic data. Values of ΔE= 77330 J/kmol and k_d^o = 8.06 kmol/Pa/s/m^2 were suggested by Clarke and Bishnoi (2001).

If hydrate is of the form, $CH4-(N_H)H_2O$, where N_H corresponds to the number of water molecules in the hydrate, then the rates of mass generation for water and the rate of reduction of hydrate mass are given as

$$\dot{m}_w = M_w N_H \dot{m}_g / M_g \tag{22}$$

$$-\dot{m}_H = M_H \dot{m}_g / M_g \tag{23}$$

where M_g, M_w and M_H are molecular weights of gas, water and hydrate phases.
For hydrate in a porous medium with saturation $S_{H,}$ assuming hydrate are formed as spherical particles having a surface area A_{HS}, the total surface area of hydrate per unit volume of the porous medium (A_p) is $\phi_o S_H A_{HS}$. Then, the mass generation rate of gas and water per unit volume of the porous medium by hydrate dissociation are given by

$$\dot{m}_g = k_B M_g A_{HS} \phi_o S_H \left[P_e(T) - P\right], \quad P \le P_e \tag{24}$$

The heat of hydrate dissociation is given as (Masuda et al., 1999)

$$\dot{Q}_H = \frac{-\dot{m}_H (c + dT)}{M_H}, \tag{25}$$

where c = 56,599 J/mol, d = -16.744 J/mol.K.

5. Core Simulation Results

An axisymmetric computational model for analyzing the dissociation of a sandstone hydrate core is described in this section and the corresponding multiphase flows of water and gas are discussed. The core is assumed to be 30.0 cm in length and 5.1 cm in diameter. The computational model was created in Gambit pre-processor, and was meshed using structured rectangular cells. A computational mesh with 800 cells is used. The core is assumed porous with variable porosity. The local relative permeability of water and gas are also allowed to vary with time as hydrate dissociates. An ideal gas model for the gas phase is assumed and the Volume of Fluid (VOF) model is used for simulation of water and gas flows.
A pressure outlet boundary condition was defined on the right side of the core, which represented the opening of outlet valve. On all walls, no-slip boundary condition was assumed. Free convection heat transfer between all the walls of the core and the surrounding was also assumed. In this section, the simulation results for five different cases are presented.
Figure 6 shows the time evolution of the static pressure contours in the core sample at different times after the outlet valve opens. This figure shows that the pressure in the core gradually decreases from an initial value of 3.75 MPa to the outlet pressure of 2.84 MPa. Hydrate dissociation is initiated as soon as the pressure in the core sample becomes less than the equilibrium pressure. Then the generated gas and water begin to move toward the outlet valve. The low-pressure front continues to move from the outlet valve into the core sample causing the hydrate to dissociate along the core. After 200 minutes, Figure 2d shows that the pressure in the core reaches to about the surrounding pressure.

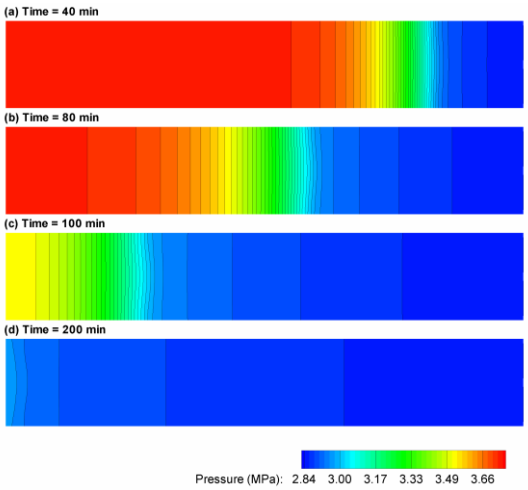

Figure 6. Pressure contours in the core sample at different times.

Figure 7 displays the contours of temperature in the core sample at four different times. The core sample is assumed to be in air with constant temperature. The temperature at the outlet valve is the same as the surrounding air temperature. Free convection heat transfer between the core walls and the surrounding is included in the model. As noted before, hydrate dissociation is an endothermic process, which results in absorption of heat. Figure 7 shows that as hydrate in the core sample dissociates, heat is absorbed from the surrounding, which results in decreasing the local temperature in the core. The low temperature regions in Figure 7 represent the areas that hydrate is dissociating. As noted before, hydrate dissociation generates natural gas and liquid water that flow toward the outlet valve. Natural convection heat transfer increases the temperature of the core sample on the right hand side of the dissociation region (toward the outlet valve). Figure 7d shows that the core temperature approaches the surrounding air temperature with time.

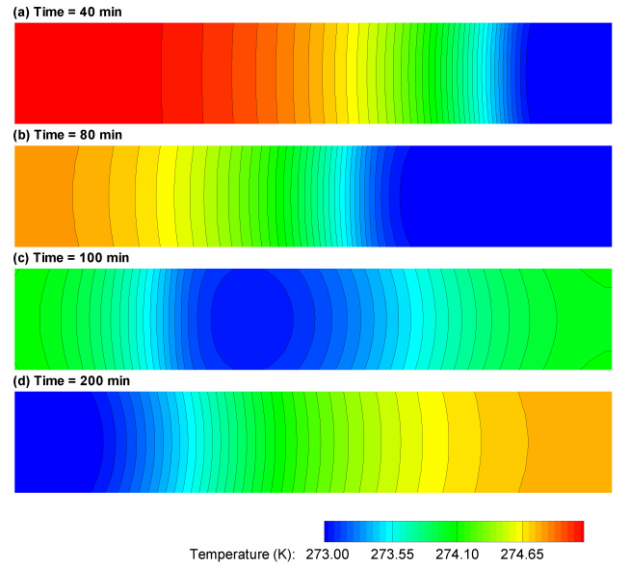

Figure 7. Temperature contours in the core sample at different times.

Figures 8 and 9, respectively, display the saturation contours of hydrate and gas in the core sample at different times. The contour plot for water saturation is very similar to that of gas

and is not shown here. The initial values of saturations in the core sample are listed in Table 1. Figure 8 shows that hydrate dissociation starts from the outlet valve where the pressure is lower than the equilibrium pressure. The dissociation front is roughly planar at the initiation of the dissociation process. As the front moves away from the outlet region it develops a curvature due to the non-uniformity of the temperature field. Figure 8d shows that the majority of hydrate is dissociated after 200 minutes. As hydrate dissociates, methane and water are generated. From Figure 9 it is seen that the saturations of methane increase as the saturation of hydrate in the core sample decreases due to dissociation.

Table 1 – Initial Conditions.

Core Temperature (K)	275.45
Initial Pressure (MPa)	3.75
Initial Hydrate Saturation	0.465
Initial Water Saturation	0.351
Initial Gas Saturation	0.206
Initial Porosity	0.182
Initial Absolute Permeability (mD)	97.98

6. Comparison with Experimental Data

Masuda et al. (1999) have reported several experiments on dissociation of hydrate in a vessel that is similar to the present core sample. They have reported their approximate initial saturations for gas, hydrate and water in their experiment, which are listed in Table 1. For the simulation, we have used the identical values of the parameters and resulting simulation results are compared with Masuda et al. experimental data in this section.

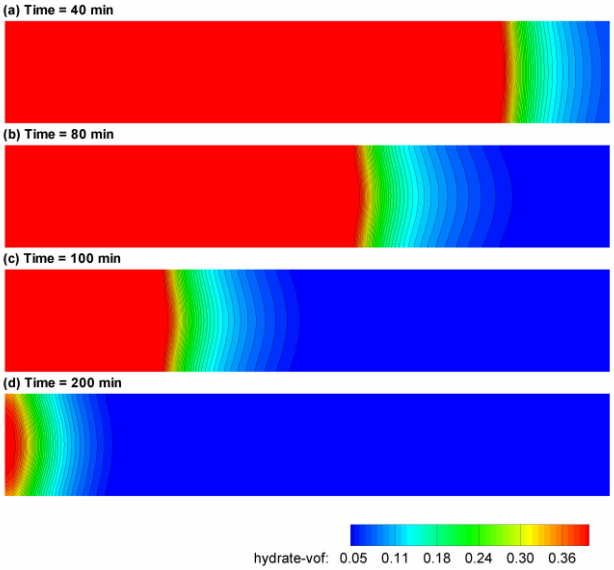

Figure 8. Hydrate saturation contours at different times.

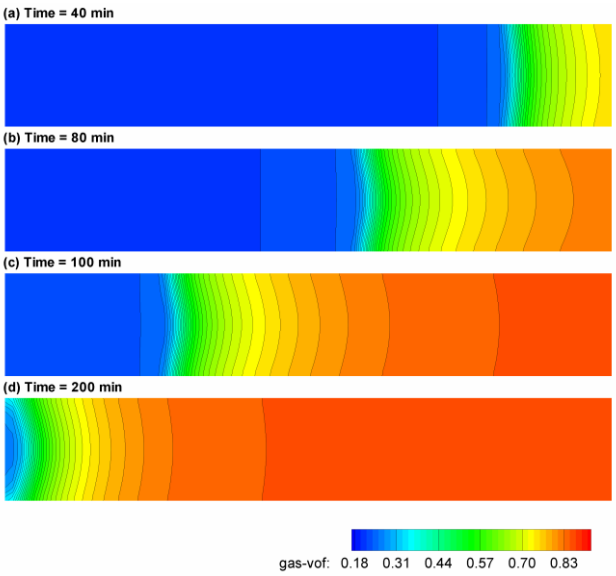

Figure 9. Methane gas saturation contours at different times.

Figure 10 shows the simulated time variations of the temperature at different sections of the core. Here the simulated temperatures are averaged across the respective sections. The experimental data for time variation of temperature as reported by Masuda et al. (1999) are shown in this figure for comparison. It is seen that the simulation results are in good agreement with the experimental data. The temperatures in all sections of the core sample for both simulation and experimental data decreases to a minimum as hydrate dissociates and then increases and approaches the surrounding temperature. As noted before, hydrate dissociation is an endothermic process and absorbs heat that causing the drop in the temperature. The free convection heat transfer then causes the core temperature to approach the surrounding air temperature.

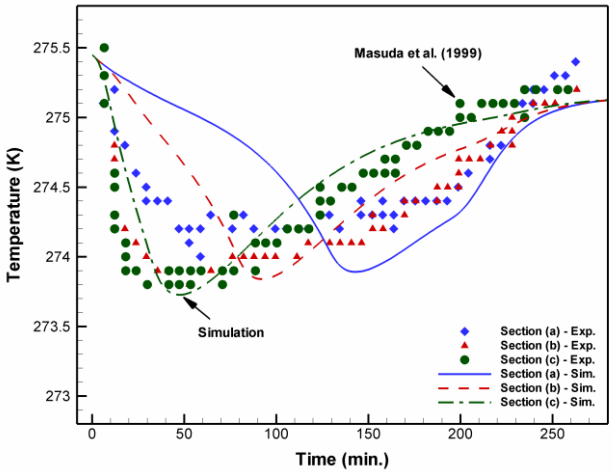

Figure 10. Comparison of temperature variations from simulation to experimental data.

Figure 11 compares the cumulative gas generated as predicted by the present simulation and the experimentally measured values of Masuda et al (1999). This figure shows the predicted monotonically increasing trend in the cumulative gas generation is comparable to that of the

experimental data. The simulation predicts that the core sample generates about 9014 standard cm^3 of methane gas when all the hydrate in the core dissociates. Masuda et al. (1999), however, reported generation of about 9067 standard cm^3 of methane gas, which is slightly higher than the simulation results.

7. Conclusions

Computational modeling of hydrate dissociation was described. A simplified axisymmetric model for natural gas production from the dissociation of methane hydrate in a confined reservoir by a depressurizing well was first described. The axisymmetric governing equations for pressure and temperature fields in the reservoir, as well as balance of energy and mass flows at the dissociation front are solved using a finite difference method in conjunction with an iterative scheme. Time evolutions of temperature, pressure, gas mass flow and heat flux profiles across the reservoir, as well the movements of dissociation front and the natural gas output are evaluated. The results are compared with those of the linearization method suggested by Makogon (1997) and Ji et al. (2001).

For the second approach, the dissociation of methane hydrate in a porous core sample including methane gas and water generations as well as the thermal and multiphase flow conditions were studied. The ANSYS-FLUENT code augmented with a newly developed Users' Defined Functions (UDF) was used in the analysis. An axisymmetric model of the core was formulated and solved. The corresponding multiphase gas-liquid flows during hydrate dissociation process were analyzed. For different surrounding temperatures and various outlet valve pressures, time evolutions of gas and water generations during hydrate dissociation were evaluated and variations of temperature and pressure and flow conditions in the core were simulated. The simulation results were compared with the experimental data of Masuda et al. (1999) and favorable agreement was observed. On the basis of the results presented, the following conclusions are drawn:

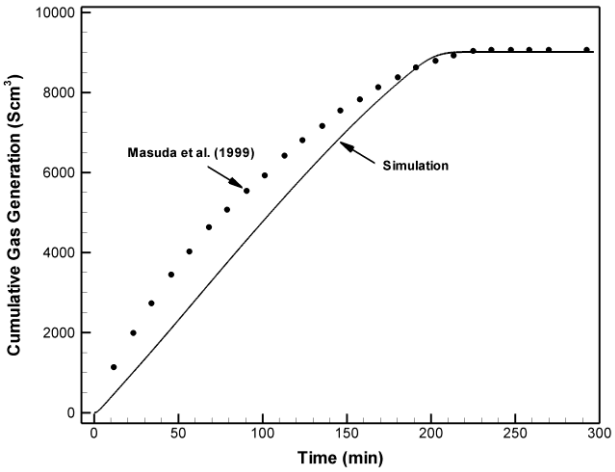

Figure 11. Comparison of cumulative gas generation with the experimental data.

1. Under some conditions, depressurization by a drilling well may be a viable method for producing natural gas from a hydrate reservoir.
2. The well pressure controls the rate of natural gas output and the motion of the dissociation front.
3. The natural gas output and the movement of the dissociation front are also sensitive functions of reservoir temperature.

4. The dissociation temperature and pressure are slowly varying functions of time.
5. A higher well pressure or a higher reservoir temperature leads to a higher dissociation temperature and pressure.
6. Compared to the linearization method used in Makogon's model, the numerical method provides a more accurate description for the process of hydrate dissociation.
7. Porosity and relative permeability are important factors affecting the hydrate dissociation and gas generation processes.
8. For the core sample studied, the temperature near the dissociation front decreases due to hydrate dissociation and then increases due to thermal convection.
9. Increasing the surrounding temperature increases the rate of gas and water production due to faster rate of hydrate dissociation.
10. Decreasing the outlet valve pressure increases the rate of hydrate dissociation and therefore the rate of gas and water production increases.
11. The developed Users' Defined Function for the Fluent Code provides a reasonable tool for computational modeling of hydrate dissociation in core samples.

Acknowledgement
The supports of the Office of Fossil Energy, U.S. Department of Energy and Clarkson University are gratefully acknowledged.

References

1. Ahmadi, G., Ji, C. and Smith, D.H., 2004, Numerical solution for natural gas production from methane hydrate dissociation, Journal of Petroleum Science and Engineering, Vol. 41, pp. 269-285.
2. Ahmadi, G., Ji, C. and Smith, D.H., 2007, Natural gas production from hydrate dissociation: An axisymmetric model, Journal of Petroleum Science and Engineering, (In Press).
3. Clarke, M. and Bishnoi, P.R., 2000, Determination of the intrinsic rate of ethane gas hydrate decomposition, Chemical Engineering Science, Vol. 55, pp. 4869-4883.
4. Clarke, M.A., Pooladi-Darvish, M. and Bishnoi, P.R., 1999, A method to predict equilibrium conditions of gas hydrate formation in porous media, Industrial and Engineering Chemistry Research, Vol. 38, pp. 2458-2490.
5. Collett, T. S., 2002, Energy resource potential of natural gas hydrates, AAPG Bulletin, v. 86, pp. 1971-1992.
6. Collett, T.S. and Kuskra, V.A., 1998, Hydrates contain vast store of world gas resources, Oil and Gas J., Vol. 96, pp. 90-95.
7. Collett, T. S., 1997, Gas hydrate resources of northern Alaska,: Bull. Canadian Petrol. Geol., Vol. 45, pp. 317-338.
8. Collett, T. S., 1993, Natural gas hydrates of the Prudhoe Bay and Kuparuk River area, North Slope, Alaska: AAPG Bulletin, Vol. 77, pp. 793-812.
9. Collett, T. S., 1993, Natural gas production from Arctic gas hydrates, U.S. Geological Survey Professional Paper 1570, Washington, United States Government Printing Office, pp. 299-311.
10. Davidson, D., 1983, Gas hydrates as clathrate ices, in Cox, J., ed., Natural gas hydrates--properties, occurrence and recovery, Butterworth, Woburn, MA, pp. 1-16.
11. Englezos, P., 1993, Reviews: Clathrate Hydrates, Ind. Eng. Chem. Vol. 32. pp.1251-1274.

12. Englezos, P. and Hatrikiriakos, S.G., 1994, Environmental aspects of clathrate hydrates, International conference on natural gas hydrates proceeding, Annals of the New York Academy of Science, Vol. 715, pp. 270-282.

13. Englezos, P., Kalogerakis, N. and Bishnoi, P.R., 1993, A Systematic Approach for the Efficient Esation of EOS Interaction Parameters using Binary VLE Data, Can. J. Chem. Eng., Vol. 71 , pp. 322-326.

14. Englezos, P., N. Kalogerakis and Bishnoi, P.R., 1990, Natural gas hydrate formation and decomposition, Journal of Inclusion Phenomena, and Molecular Recognition in Chemistry, Vol. 8, pp. 89-101.

15. Englezos, P. and Bishnoi, P.R., 1988, Gibbs free energy analysis for the supersaturation limits of methane in liquid water and the hydrate-gas-liquid water phase behaviour, Fluid Phase Equilibria, Vol. 42, pp. 129-140.

16. Englezos, P. and Bishnoi, P.R., 1988, Prediction of gas hydrate formation conditions in aqueous electrolyte solutions, A.I.Ch.E. J., Vol. 34, pp. 1718-1721.

17. Englezos, P., Kalogerakis, N., Dholabhai, P.D. and Bishnoi, P.R., 1987, Kinetics of gas hydrate formation from mixtures of methane and ethane, Chem. Eng. Sci., Vol. 42, pp. 2659-2666.

18. Englezos, P., N. Kalogerakis, P.D. Dholabhai and P.R. Bishnoi, 1987, Kinetics of Formation of Methane and Ethane Gas Hydrates, Chem. Eng. Sci., Vol. 42, pp. 2647-2658.

19. Goel, N., M. Wiggins, and S. Shah, 2001, Analytical modeling of gas recovery from in situ hydrates dissociation, J. of Petroleum Science and Engineering, Vol. 29, pp. 115-127.

20. Haq, B. U., 1998, Natural gas hydrates: searching for the long-term climatic and slope-stability records, London, The Geological Society, Spec. Publication 137, pp. 303-318.

21. Henriet, J.-P., 1998, Gas Hydrates: Relevance to World Margin Stability and Climate Change, Gas Hydrates, Relevance to World Margin Stability and Climate Change, London, The Geological Society, Special Publications.

22. Hesselbo, S. P., D. R. Gröcke, H. C. Jenkyns, C. J. Bjerrum, P. Farrimond, H. S. Morgans Bell, and O. R. Green, 2000, Massive dissociation of gas hydrate during a Jurassic oceanic anoxic event: Nature, Vol. 406, pp. 392-395.

23. Holder, G.D., Mokkaa, L.P., Warzinskib, R.P., 2001. Formation of gas hydrates from single-phase aqueous solutions, Chem. Eng. Sci., Vol. 56, pp. 6897-6903.

24. Holder, G.D., Angert, P.F., John, V.T., et al., 1982. A thermodynamic evaluation of Thermal recovery of gas from hydrates in the Earth, J. Petrol. Technology, Vol. 34, pp. 1127-1132.

25. Hong, H. and Pooladi-Darvish, M., 2003a, A Numerical Study on Gas Production from Formations Containing Gas Hydrates, paper CIPC 2003-60 presented at the 2003 CIPC Conference, Calgary.

26. Hong H., Pooladi-Darvish, M., and Bishnoi, P.R., 2003b, Analytical Modeling of Gas Production from Hydrates in Porous Media, J. Canadian Pet. Tech., Vol. 42, pp. 45-56.

27. Jamaluddin, A.K., Kalogerakis, N., and Bishnoi, P.R.: Modeling of Decomposition of a Synthetic Core of Methane-Gas Hydrate by Coupling Intrinsic Kinetics with Heat-Transfer Rates, Canadian. J. Chemical Engineering, December 1989, Vol. 67, pp. 948-954.

28. Ji, C., Ahmadi, G. and Smith, D.H., 2001, Natural gas production from hydrate decomposition by depressurization, Chemical Engineering Science, Vol. 56, pp. 5801-5814.

29. Ji, C., Ahmadi, G. and Smith, D.H., 2003, Constant rate natural gas production from a well in a hydrate reservoir, Energy Conversion and Management, Vol. 44, pp. 2403-2423.

30. Ji, C., Ahmadi, G., and Smith., D.H., (2002) "Numerical Solution for Natural Gas Production from Methane Hydrate Dissociation: A One-Dimensional Model, " submitted for publication.
31. Kalogerakis, N., Jamaluddin, A.K.M., Dholabhai, P.D. and Bishnoi, P.R., 1993, Effect of Surfactants on Hydrate Formation Kinetics, Society of Petroleum Engineers, SPE-25188.
32. Kamath, V., (1983) "Study of Heat Transfer Characteristics During Dissociation of Gas Hydrates in Porous Media," Ph.D. Thesis, University of Pittsburgh, Pittsburgh, PA.
33. Kamath, V.A., 1998, A Perspective on Gas Production from Hydrates, paper presented at the JNOC's Methane Hydrate Intl. Symposium, Chiba City, Japan.
34. Kim, H.C., Bishnoi, P.R., Heidemann, R.A and Rizvi, S.S.H., 1987, Kinetics of Methane Hydrate Decomposition, Chemical Engineering Science, Vol. 42, pp. 1645-1653.
35. Kneafsey, T. J., Tomutsa, L., Moridis, G. J., Seol, Y., Freifeld, B., Taylor, C. E. and Gupta, A., 2005, Methane Hydrate Formation and Dissocation in a Partially Saturated Sand--Measurements and Observations, Lawrence Berkeley National Laboratory, LBNL-57300.
36. Kvenvolden, K. A., 1994, Natural Gas Hydrate Occurrence and Issues, International Conference on Natural Gas Hydrates, Annals of the New York Academy of Sciences, pp. 232-246.
37. Kvenvolden, K. A., 1993. Gas Hydrate:Geological Perspective and Global Change. Reviews Geophysics, Vol. 31, pp. 173-187.
38. Kvenvolden, K. A., 1993, Gas hydrates as a potential energy resource - a review of their methane content, U.S. Geological Survey Professional Paper 1570: Washington, United States Government Printing Office, pp. 555-561.
39. Kvenvolden, K. A., 1993, A primer on gas hydrates, in D. G. Howell, ed., The Future of Energy Gases, U.S. Geological Survey Professional Paper 1570: Washington, United States Government Printing Office, pp. 279-291.
40. Kvenvolden, K. A., 1991, A review of Arctic gas hydrates as a source of methane in global change, International Conference on the Role of the Polar Regions in Global Change, Geophysical Institute and Center for Global Change and Arctic System Research, University of Alaska Fairbanks, pp. 696-701.
41. MacDonald, G.J., 1990a, Role of methane clathrates in past and future climates: Climatic Change, Vol. 16, pp. 247-281.
42. MacDonald, G.J., 1990b, The future of methane as an energy resource: Annual Review of Energy, Vol. 15, pp. 53-83.
43. Makogon, Y. F., 1974. Hydrates of Natural Gas, Penn Well Publishing, Tulsa, OK.
44. Makogon, Y.F., 1997, Hydrates of natural gas, Penn Well Books, Tulsa, OK.
45. Makogon, Y.F., 1981, Hydrates of natural gas, Penn Well Books, Tulsa, Oklahoma.
46. Masuda, Y., Fujinaga, Y., Naganawa, S., Fujita, K., Sato, K. and Hayashi, Y., 1999, Modeling and Experimental Studies on Dissociation of Methane Gas Hydrates in Berea Sandstone Cores, Proc., 3rd Intl. Conference on Gas Hydrates, Salt Lake City, Utah, U.S.A.
47. Milkov, A. V. and R. Sassen, 2003, Preliminary assessment of resources and economic potential of individual gas hydrate accumulations in the Gulf of Mexico continental slope, Marine and Petroleum Geology, v. 20, pp. 111-128.
48. Moridis, G. J., Seol, Y. and Kneafsey, T. J., 2005, Studies of Reaction Kinetics of Methane Hydrate Dissociation in Porous Media", Lawrence Berkeley National Laboratory, LBNL-57298.

49. Paez, J. E., R. Blok, H. Vaziri, and M. R. Islam, 2001, Problems in Gas Hydrates: Practical Guidelines for Field Remediation, Society of Petroleum Engineers, SPE-69424.

50. Reyma, E., and S. Stewart, 2001, Case History of the Removal of a Hydrate Plug Formed During Deep Water Well Testing, Society of Petroleum Engineers, SPE-67746.

51. Selim, M.S. and Sloan, E.D., 1990, Hydrate Dissociation in Sediment, Society of Petroleum Engineers, SPE-16859.

52. Sloan, E.D., 1998, Clathrate Hydrate of Natural Gases, Marcel Dekker, New York.

53. Sun, X. and Mohanty, K.K., 2006, Kinetic Simulation of Methane Hydrate Formation and Dissociation in Porous Media, Chemical Engineering Science, Vol. 61, pp. 3476 – 3495.

54. Vysniauskas, A. and Bishnoi, P.R., 1985, Kinetics of ethane hydrate formation, Chem. Eng. Sci., Vol. 40, pp. 299-303.

55. Vysniauskas, A. and Bishnoi, P.R., 1983, A kinetic study of methane hydrate formation, Chem. Eng. Sci., Vol. 38, pp. 1061-1072.

56. Yousif, M., and V. Dunayevsky, 1997, Hydrate Plug Remediation: Options and Applications for Deep Water Drilling Operations, Society of Petroleum Engineers, SPE/IADC 37624.